Thwaites Glacier grounding-line retreat: influence of width and buttressing parameterizations

David DOCQUIER,[1] David POLLARD,[2] Frank PATTYN[1]

[1]*Laboratoire de Glaciologie, Université Libre de Bruxelles, Brussels, Belgium*
E-mail: docquier.david@gmail.com
[2]*Earth and Environmental Systems Institute, The Pennsylvania State University, University Park, PA, USA*

ABSTRACT. Major ice loss has recently been observed along coastal outlet glaciers of the West Antarctic ice sheet, mainly due to increased melting below the ice shelves. However, the behavior of this marine ice sheet is poorly understood, leading to significant shortcomings in ice-sheet models attempting to predict future sea-level rise. The stability of a marine ice sheet is controlled by the dynamics at the grounding line, the boundary between the grounded ice stream and the floating ice shelf. One of the largest contributors to current sea-level rise is the fast-flowing Thwaites Glacier, which flows into the Amundsen Sea. Here we use an ice-stream/ice-shelf model and perform a number of experiments along a central flowline to analyze the sensitivity of its grounding line on centennial timescales. In the absence of width and buttressing effects, we find that the grounding line retreats by ~300 km in 200 years from the present day (rate of 1.5 km a^{-1}). With variable glacier width implemented in the model, flow convergence slows the retreat of Thwaites grounding line at 0.3–1.2 km a^{-1}. The parameterization of ice-shelf buttressing according to different observed scenarios further reduces the glacier retreat and can even lead to a slight advance in the most buttressed case.

KEYWORDS: glacier flow, ice dynamics, ice-sheet modelling

INTRODUCTION

Recent satellite observations and techniques, such as satellite laser altimetry, time-variable gravity and the mass-budget method, have shown that the West Antarctic ice sheet (WAIS) has been losing ice at a considerable rate over recent decades (Rignot and others, 2008, 2011; Chen and others, 2009; Pritchard and others, 2012). The primary trigger of this recent loss appears to be increased sub-ice-shelf melt. A likely shift in wind patterns has resulted in the delivery of substantial volumes of Circumpolar Deep Water underneath the floating ice shelves of the Amundsen Sea Embayment (ASE) (Thoma and others, 2008; Pritchard and others, 2012). The subsequent high basal melt rates lead to a thinning of the ice shelves, which reduces their restraint (the so-called 'buttressing effect') on inland glaciers (Dupont and Alley, 2005). Loss of buttressing has increased the flow rate of inland outlet glaciers and thus grounded ice-sheet loss, contributing to sea-level rise (Rignot and others, 2011).

The WAIS has a bed that is grounded well below sea level and generally sloping upward toward the ocean (known as a 'retrograde' bed slope; Gudmundsson and others, 2012). In such a situation, the grounding line, defined as the boundary between the grounded ice sheet and the floating ice shelf, is unstable if the ice shelf is freely floating, at least in flowline models with no transverse variations (Weertman, 1974; Schoof, 2007). Attention has been paid to the WAIS due to this possible marine ice-sheet instability and to the observational evidence that glaciers have been retreating inland. Gudmundsson and others (2012) have found stable steady-state grounding-line positions on retrograde bedrock slopes using a three-dimensional (3-D) ice-sheet model, due to the presence of ice-shelf buttressing, but the bedrock configuration of these experiments is very specific and would not necessarily lead to ice-sheet stability if slightly modified.

Located in the ASE, Thwaites Glacier (TG) is one of the largest, fastest-flowing and fastest-thinning glaciers of the WAIS. Together with Pine Island Glacier (PIG), it drains ~20% of the WAIS and significantly contributes to current Antarctic ice-sheet loss and thus sea-level rise (Rignot and others, 2008). Thwaites Glacier has two distinct floating ice masses: the TG tongue, downstream of the central area of fastest flow and providing limited buttressing to the inland ice (Rignot, 2008; Parizek and others, 2013), and the eastern ice shelf, where the velocities are much lower than in the tongue, due to the presence of a pinning point (Tinto and Bell, 2011). In 2010, a major part of the TG tongue calved, although there is still an ice melange linking the new iceberg (>2000 km^2) and the smaller remaining ice tongue (MacGregor and others, 2012). If the eastern ice shelf was to calve, as the TG tongue did in 2010, the buttressing provided by the pinning point would be lost.

Motivated by the relatively small number of modeling studies on TG (described below), combined with its potential contribution to future sea-level rise, we performed sensitivity experiments using a variety of datasets (geometry, ice velocity, basal shear stress, ice temperature, sub-ice-shelf melt rate, accumulation rate) that we incorporated into a finite-difference flowline ice-stream/ice-shelf shallow-shelf approximation (SSA) model. The data, the model and the different sensitivity experiments are described below. We also present the results of our modeling study as well as a discussion.

PREVIOUS MODELING STUDIES

Several modeling efforts have been carried out on PIG, but there has been less attention paid to TG to date. The 3-D SSA model of Joughin and others (2010a) indicated that the grounding-line retreat rate of PIG should diminish soon, but

https://doi.org/10.3189/2014JoG13J117 Published online by Cambridge University Press

the glacier would continue to lose mass at rates comparable with the present. In another study of PIG, Gladstone and others (2012) coupled their flowline SSA model to an ice-shelf cavity circulation model (Olbers and Hellmer, 2010), predicting a monotonic retreat of the grounding line over the next 200 years, with large uncertainty in the retreat rate. They used parameterized mass balance and basal friction coefficients, and constant Glen's flow law parameter and channel width. Cornford and others (2013) applied their 3-D depth-integrated hybrid finite-volume model with adaptive mesh refinement to PIG and showed a rapid deglaciation caused by sub-ice-shelf melting.

Concerning TG, a recent modeling study by Parizek and others (2013) focused on the impact of spatial resolution of existing datasets, grounding-zone processes and till rheology on the glacier dynamics. They used an ice-stream/ice-shelf finite-element model with 1.5- and 2.5-D treatments of mass continuity and momentum balance, respectively, coupled to an ocean-plume model. They applied the model in flowline mode to the center line of TG. They showed that a bedrock rise, currently located upstream of the grounding line, produces a stable grounding-line position for centuries or longer. This stabilization disappears and TG retreats if the basal friction is reduced and warm water penetrates into the grounding zone, unless the bed is effectively plastic.

The approach taken here differs from that of Parizek and others (2013) in three ways. First, the domain extends upstream all the way to the ice divide, while Parizek and others (2013) started the domain at the confluence of TG tributaries, where incoming ice flux is specified as a boundary condition. Second, we use the recent bathymetry of Tinto and Bell (2011) and also test the new bed data from Bedmap2 (Fretwell and others, 2013). Third, we focus on variable-width and buttressing parameterizations.

METHODOLOGY

Data

We used the following elevation, ice thickness and bathymetry datasets as input into our model: (1) ice surface elevation of Bamber and others' (2009) 1 km digital elevation model; (2) grounded ice thickness interpolated from the work of Holt and others (2006) and Le Brocq and others (2010); (3) floating ice thickness derived from Bamber and others (2009), using a hydrostatic assumption (Griggs and Bamber, 2009); and (4) bathymetry from Nitsche and others (2007) and Le Brocq and others (2010), with the addition of the Tinto and Bell (2011) bathymetric model.

We used surface velocity, u, and basal shear stress, τ_b, from Joughin and others (2009) to calculate the basal friction coefficient, C, using a Weertman-type sliding law:

$$C = \frac{\tau_b}{|u|^{m-1}u}, \quad (1)$$

where m is the basal friction exponent. No consensus has emerged on the most realistic value of m (Gudmundsson, 2011). In our study, m is set to 1/3, based on prior model experiments with m values in the range 1/8 to 1, seeking the best match with observed modern velocities.

Ice temperature and sub-ice-shelf melt rate are prescribed from the modern output of another 3-D ice-sheet/ice-shelf model (Pollard and DeConto, 2012). We derived Glen's flow parameter, A, from ice temperature using eqn (16) of Pollard and DeConto (2012) and sub-ice-shelf melt rate from Pollard and DeConto's (2012) eqn (17). We used estimates of accumulation rate from Van de Berg and others (2006).

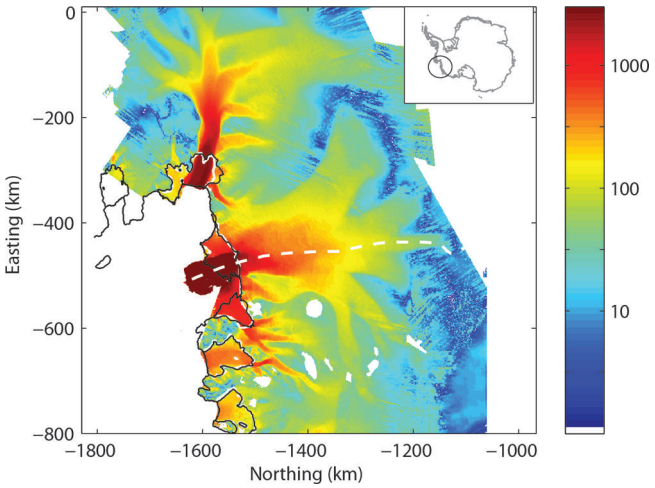

Fig. 1. Observed ice velocity (m a^{-1}) of the ASE (Joughin and others, 2009), with the flowline of Thwaites Glacier used in this study represented as a dashed white curve and the Mosaic of Antarctica (MOA) grounding line shown in solid black (Scambos and others, 2007). The inset shows the location of the ASE in Antarctica.

All of the input data (elevation, ice thickness, velocity, basal shear stress, Glen's flow parameter, sub-ice-shelf melt rate and accumulation rate) were interpolated onto our model grid.

We use the same flowline coordinates as Parizek and others (2013), which represent the line of fastest flow. Figure 1 shows the flowline used in this study, superimposed on the ice velocity map of the ASE (Joughin and others, 2009). The flowline domain length from the ice divide to the calving front is ~580 km. The geometry and velocity profiles derived from the data are shown in Figure 2a, where we can clearly identify the different bedrock highs and lows, as well as the overall upward-sloping bedrock. In contrast to Bedmap2 (Fretwell and others, 2013), our bathymetry identifies a trough in bed elevation under the ice shelf 500 km from the ice divide (Fig. 2b), which can also be seen in Tinto and Bell's (2011) figure 3b. Other differences in bed elevation (up to 200 m) between both datasets are visible upstream of the grounding line. Since Bedmap2 does not incorporate the recent bathymetric model of Tinto and Bell (2011) and its different features, we use the dataset from Tinto and Bell (2011). The grounding line of TG is located on a small sill ~450 km from the ice divide; with Bedmap2 topography, the grounding line would be 5 km downstream of this sill on a downward-sloping bed (Fig. 2). Therefore, simulations using Bedmap2 data would have a slower retreat due to the more stable initial grounding-line position (Schoof, 2007).

Model description

We use a finite-difference flowline ice-stream/ice-shelf model (vertically integrated) that computes the SSA on a fixed staggered grid, with x and z being the distance along the flow from the ice divide to the calving front and the elevation above sea level, respectively. The model is the SSA–FG model, which stands for 'shallow-shelf approximation – fixed grid', as used by Drouet and others (2013). This model has successfully participated in the Marine Ice Sheet

https://doi.org/10.3189/2014JoG13J117 Published online by Cambridge University Press

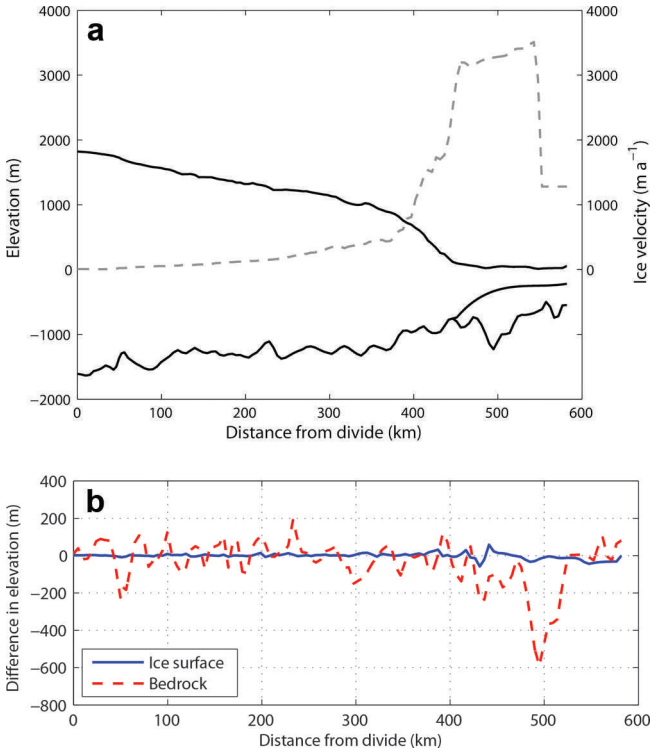

Fig. 2. (a) Observed geometry (solid black curves) and ice velocity (dashed gray curve) profiles of Thwaites Glacier from the ice divide to the calving front with our dataset. (b) Difference in ice surface and bedrock elevations between our dataset and Bedmap2.

Model Intercomparison Project (MISMIP; Pattyn and others, 2012) under the name 'FPA5'. The grid size needs to be small enough to enable an accurate calculation of the motion of the grounding line (Vieli and Payne, 2005; Durand and others, 2009; Docquier and others, 2011; Pattyn and others, 2012, 2013). In this study, we use a grid size of 50 m.

The use of such a flowline model, instead of a 3-D model, is justified by the fact that some 3-D effects can be parameterized (such as the buttressing effect and the flow convergence) and the computation time is much shorter than with a 3-D full-Stokes model.

We assume that the SSA can be used to simulate the behavior of fast-flowing glaciers, such as TG. In the most upstream regions of the drainage basin, vertical shear stress may play a more important role, but we did not take it into account, due to the lack of corresponding studies.

The horizontal velocity, u, is obtained by solving the following SSA equations (Eqns (2) and (3)) (MacAyeal, 1989). In the grounded ice sheet ($0 \leq x \leq x_g$), basal friction is taken into account:

$$2\frac{\partial(h\tau_{xx})}{\partial x} - Cu^m = \rho_i g h \frac{\partial z_s}{\partial x}, \quad (2)$$

and in the floating ice shelf ($x_g < x \leq x_f$):

$$2\frac{\partial(h\tau_{xx})}{\partial x} = \gamma h \frac{\partial h}{\partial x}, \quad (3)$$

where x_g is the grounding-line position, x_f is the calving front position, h is the ice thickness, $\tau_{xx} = 2\eta\partial u/\partial x$ is the longitudinal deviatoric stress, ρ_i is the ice density, g is the gravitational acceleration and z_s is the ice surface elevation. A comparison between lateral drag (calculated as by Van der Veen and Whillans, 1996) and basal drag showed that the former is much less important than the latter for the flowline used here. Furthermore, Parizek and others (2013), who use the same flowline as in our experiments (except that it starts from the flow convergence), mention that basal drag is dominant over lateral drag in their study area. Therefore, lateral drag was not parameterized in the model. The effective viscosity, η, is computed as

$$\eta = \frac{1}{2}A^{-\frac{1}{n}}\left(\frac{\partial u}{\partial x}\right)^{\frac{1-n}{n}}, \quad (4)$$

where A and $n = 3$ are the Glen's flow law parameter and exponent, respectively; γ is defined as

$$\gamma = \rho_i g\left(1 - \frac{\rho_i}{\rho_w}\right), \quad (5)$$

where ρ_w is the water density. The boundary condition at the ice divide is $u(x = 0) = 0$, and the boundary condition at the ice bottom in the ice sheet is already included in Eqn (2). The horizontal force acting on the calving front is balanced by the hydrostatic water pressure (Paterson, 1994):

$$\frac{\partial u}{\partial x} = A\tau_{xx}^n = A\left(C_F\frac{\gamma}{4}h_f\right)^n, \quad (6)$$

where h_f is the ice thickness at the calving front and C_F is the buttressing factor (Drouet and others, 2013). A value of $C_F = 1$ means that the ice extension is opposed solely by water pressure, i.e. there is no ice-shelf buttressing. For $C_F < 1$, this induces a lower longitudinal stress at the calving front, so that the inward force at the calving front is modified by a factor C_F, simulating the buttressing effect. We model the whole ice shelf since a calving criterion is not implemented.

The ice bottom elevation, z_b, is determined from the no-penetration condition and the floating condition. For $x \leq x_g$:

$$z_b = b, \quad (7)$$

and for $x > x_g$:

$$z_b = \ell_w - h\rho_i/\rho_w > b, \quad (8)$$

where b is the bedrock elevation and ℓ_w is the sea-level height.

The ice surface elevation, $z_s = z_b + h$, is deduced from the vertically integrated mass-conservation equation, giving h as

$$\frac{\partial h}{\partial t} + \frac{1}{\omega}\frac{\partial(uh\omega)}{\partial x} = \dot{a} - \dot{m}_b, \quad (9)$$

where ω is the glacier width, $\dot{a}$ is the ice accumulation rate and $\dot{m}_b$ is the sub-ice-shelf melt rate (melting is allowed from the grounding line to the calving front). The flow convergence and divergence are therefore taken into account through the parameter ω, which varies along the flowline.

The grounding-line position is determined through the flotation criterion.

Sensitivity experiments

We performed 16 sensitivity experiments for TG (Table 1). The aim of the experiments is to investigate the behavior of TG under varying width and buttressing parameterizations, all mimicking, to some extent, possible scenarios of present-day and future states. The model is initialized using the modern observed data described above, and is then run to equilibrium with modern climate forcing. After sufficient years of integration, this yields an approximate match between observed and modeled geometry profiles on the

https://doi.org/10.3189/2014JoG13J117 Published online by Cambridge University Press

Table 1. Summary of the 16 sensitivity experiments performed at TG in this study

Exp.	Width	Buttressing
CW	Constant	$C_F = 1$
VW1	Variable (small)	$C_F = 1$
VW2	Variable (medium)	$C_F = 1$
VW3	Variable (large)	$C_F = 1$
CSW1	$\omega_s = \omega_g$	$C_F = 1$
CSW2	$\omega_s = (3\omega_g + \omega_c)/4$	$C_F = 1$
CSW3	$\omega_s = (\omega_g + \omega_c)/2$	$C_F = 1$
CF1VW3	Variable (large)	$C_F = 0.8$
CF2VW3	Variable (large)	$C_F = 0.6$
CF3VW3	Variable (large)	$C_F = 0.4$
CF4VW3	Variable (large)	$C_F = 0.2$
CF1CSW1	$\omega_s = \omega_g$	$C_F = 0.8$
CF2CSW1	$\omega_s = \omega_g$	$C_F = 0.6$
CF3CSW1	$\omega_s = \omega_g$	$C_F = 0.4$
CF4CSW1	$\omega_s = \omega_g$	$C_F = 0.2$
Bedmap2	$\omega_s = \omega_g$	$C_F = 1$

one hand, and observed and modeled velocity profiles on the other. The time-span of most experiments is 200 years, as used in 'ice2sea' projections (Gladstone and others, 2012; Hellmer and others, 2012; Drouet and others, 2013). Unless otherwise mentioned, the buttressing factor $C_F = 1$ (i.e. no ice-shelf buttressing).

In Exp. CW (Exp. and CW stand for 'experiment' and 'constant width', respectively), the glacier width is kept constant over the whole domain (which is equivalent to $\omega = 1$ in Eqn (9)), so there is no flow convergence. However, in reality, the drainage basin of TG is quite wide at the ice divide, and narrows as it approaches the ice shelf. Therefore, a spatially variable glacier width should be used in the continuity equation (Eqn (9)). This allows us to take into account the flow coming from the glacier tributaries that feed the main trunk of the glacier. Given the complex flow pattern in the interior of the TG drainage basin, several parameterizations for convergence and divergence of ice flow have been tested, which may all be plausible. Exp. VW1 (VW stands for 'variable width') has the smallest mean glacier width with diverging flow upstream of the zone of convergence noted above. Exps. VW2 and VW3 only have a convergent flow regime, with VW3 having the largest mean glacier width profile. The lateral boundaries of CW, VW1, VW2 and VW3 are shown in Figure 3a.

In the variable-width experiments (VW1–VW3), the width at the grounding line increases as the grounding line retreats inland, resulting in flow convergence within the first few kilometers of the ice shelf. This tends to generate a thicker ice shelf than is the case with constant width in the shelf. This effect may not be real, because the boundaries of shelf flow could shift laterally in different ways as the grounding line retreats. Therefore, we carry out three further experiments based on the VW3 width profile, but keeping the width in the ice shelf constant at each time-step. In these experiments, named CSW1, CSW2 and CSW3 (CSW stands for 'constant shelf width'), the ice-shelf width, ω_s, is equal to ω_g, $(3\omega_g + \omega_c)/4$ and $(\omega_g + \omega_c)/2$, respectively, where ω_g and ω_c are the widths at the current grounding line and calving front, respectively (Fig. 3b). Since the lateral boundaries of those experiments vary through time in order to keep a constant ice-shelf width, we show lateral

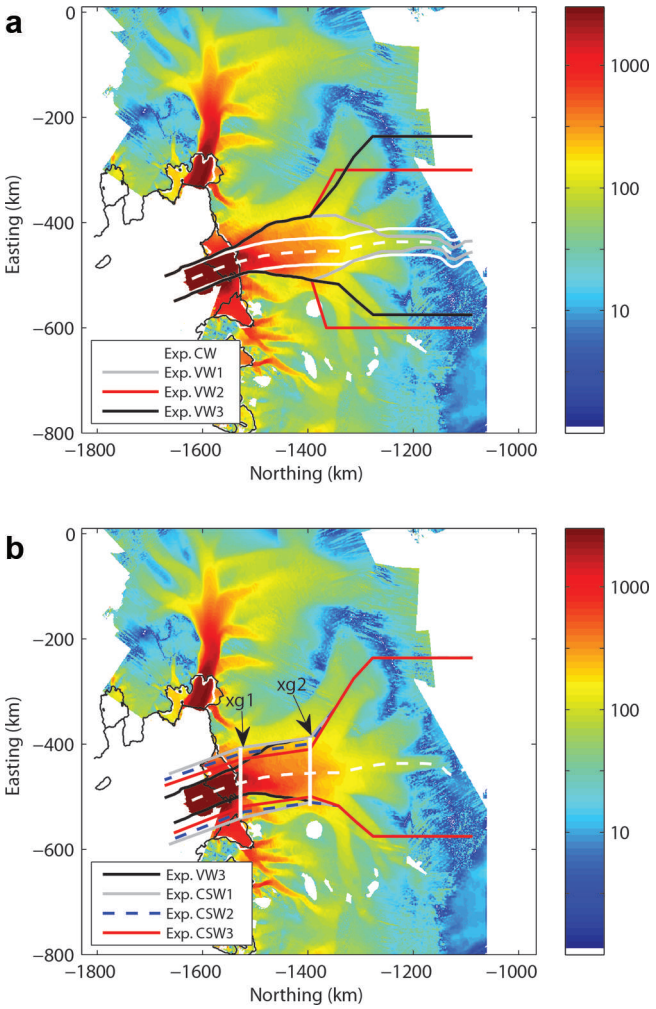

Fig. 3. Lateral boundaries of (a) Exps. CW and VW1–VW3 and (b) Exps. VW3 and CSW1–CSW3 represented in different colors. Lateral boundaries of Exps. CSW1–CSW3 correspond to the grounding-line position, xg2. The two white vertical lines in (b) are the initial grounding-line position (xg1) and the grounding-line position after ~100 years (xg2). The colored map shows the observed ice velocity (m a^{-1}) of the ASE (Joughin and others, 2009) with the flowline of Thwaites Glacier used in this study (dashed white curve) and the MOA grounding line (solid black curve) (Scambos and others, 2007).

boundaries corresponding to the middle of the simulation (after ~100 years) in Figure 3b.

Thwaites Glacier tongue is known to exert limited buttressing on the inland grounded ice (Rignot, 2008; Parizek and others, 2013), but the eastern ice shelf is in contact with a pinning point (Tinto and Bell, 2011), reducing the flow of inland ice. To simulate the buttressing effect arising from the eastern ice shelf, we reduce longitudinal stress at the calving front in Eqn (6), in a similar manner to Drouet and others (2013), i.e. by lowering the buttressing factor, C_F. Exps. CF1VW3, CF2VW3, CF3VW3 and CF4VW3 are based on the VW3 width profile and use values of $C_F = 0.8$, 0.6, 0.4 and 0.2, respectively, from the beginning of the simulation to the end. The same values of C_F are used in Exps. CF1CSW1, CF2CSW1, CF3CSW1 and CF4CSW1, which are based on the CSW1 width profile. For example, a value of $C_F = 0.2$ means that the longitudinal stress at the calving front is five times lower than if $C_F = 1$. This simulates an increase in buttressing, caused by lower

https://doi.org/10.3189/2014JoG13J117 Published online by Cambridge University Press

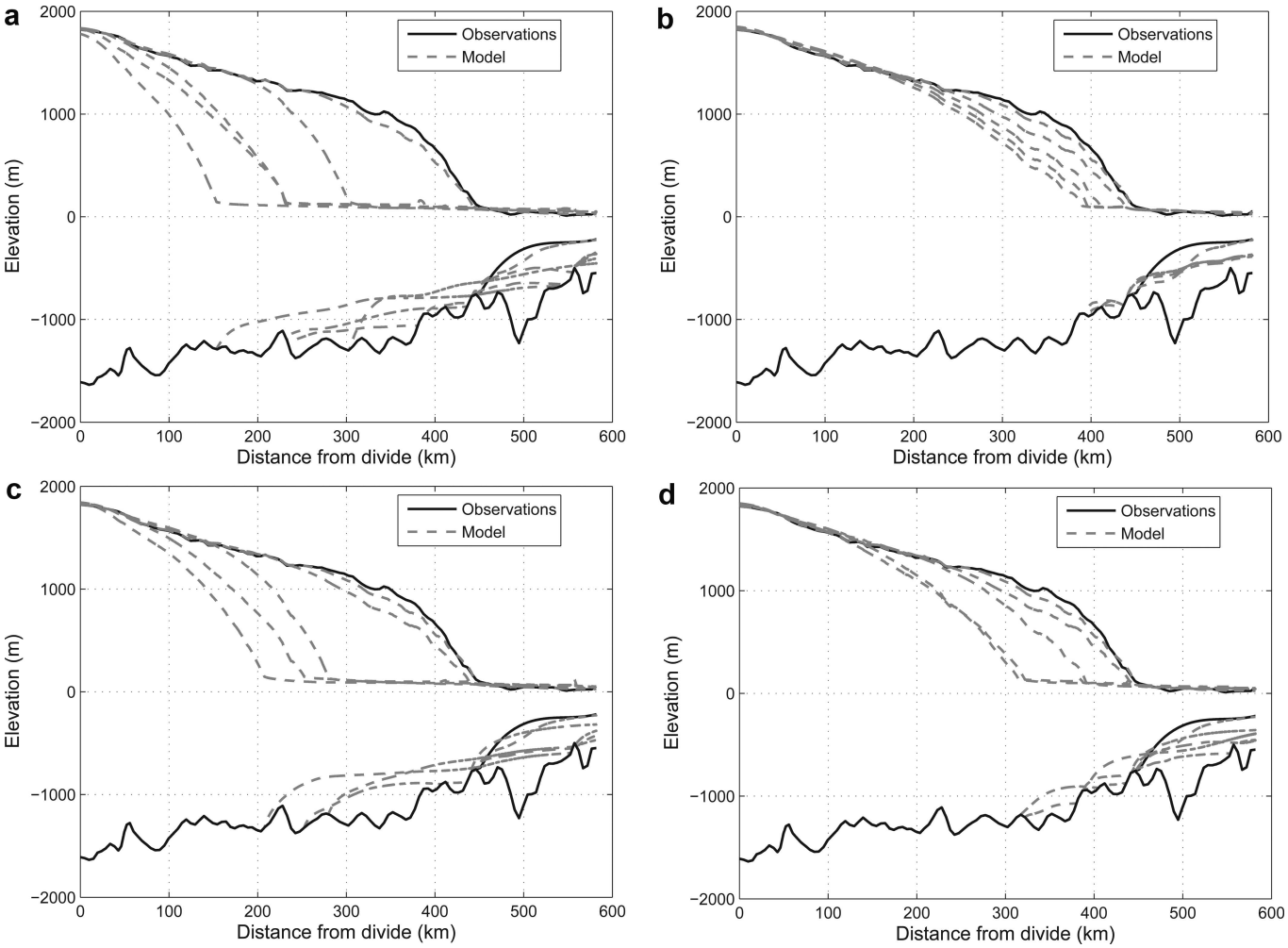

Fig. 4. Modeled geometry profiles of Thwaites Glacier after 10, 50, 100, 150 and 200 years (from right to left) and observed geometry profile for (a) Exp. CW (constant width), (b) Exp. VW3 (variable width), (c) Exp. CSW1 (constant shelf width) and (d) Exp. CF2CSW1 ($C_F = 0.6$).

sub-ice-shelf melt, for instance, and leads to deceleration of inland grounded ice.

We performed a final experiment with the new Bedmap2 bedrock data based on the CSW1 width profile to test how the new bedrock profile affects results, in comparison with the bedrock data used in the other experiments.

RESULTS AND DISCUSSION

Initialized using modern data, most of the experiments lead to an approximate match between observed and modeled geometry profiles on one hand, and observed and modeled velocity profiles on the other, after 10 model years (Figs 4 and 5).

In Exp. CW, the grounding line quickly retreats inland (Fig. 4a) and the ice-shelf velocities after 50 years reach $>10\,000\,\mathrm{m\,a^{-1}}$ (Fig. 5a is truncated at $5000\,\mathrm{m\,a^{-1}}$ to allow comparison with Fig. 5b), comparable with the maximum observed velocities of Jakobshavn Isbræ, Greenland (Joughin and others, 2004, 2010b). The grounding line is located on an overall retrograde bed slope, accelerating the glacier retreat, and reaches a position 153 km from the ice divide after 200 years. This corresponds to a mean retreat rate of $\sim 1.5\,\mathrm{km\,a^{-1}}$, higher than that observed ($1\,\mathrm{km\,a^{-1}}$; Tinto and Bell, 2011). We let the model run longer for this experiment and found that the glacier shrinks after 370 years. A contact between the ice shelf and a bedrock rise 550 km from the divide is established after 60 years, which slows the retreat for ~100 years (Fig. 6). Once the grounding line passes the bedrock rise at $x = 220\,\mathrm{km}$ (160 years), the retreat accelerates. This experiment should be considered as an end-member case, since buttressing and width variations are not included. An increase in back-stress provided by the ice shelf would slow down the grounding-line retreat (Drouet and others, 2013). A change in the width gradient from the ice divide to the calving front would also provide a slower retreat. Mathematically, the latter corresponds to a reduction of all the width terms in the discrete form of the continuity equation (Eqn (9)), reducing the ice flux at the grounding line.

Using a spatially variable glacier width in the continuity equation (Exps. VW1–VW3) slows the retreat and stabilizes the glacier at a grounding-line position of $x_g \approx 390\,\mathrm{km}$ from the ice divide after 200 years, as can be seen for Exp. VW3 in Figures 4b and 5b. The mean width rises from Exp. VW1 to VW3 (Fig. 3a), but no noticeable difference in grounding-line migration is perceived between the three experiments, due to the contact created between the ice shelf and the bedrock rise at $x = 450\,\mathrm{km}$ after 70 years (Fig. 6). The variable glacier width of these experiments takes into account the flow coming from TG tributaries (flow convergence and divergence). While the grounding line retreats, the ice-shelf width close to the grounding line increases, thereby increasing the width spatial gradient, $\partial\omega/\partial x$. Therefore, the ice shelf gets thicker and makes contact

https://doi.org/10.3189/2014JoG13J117 Published online by Cambridge University Press

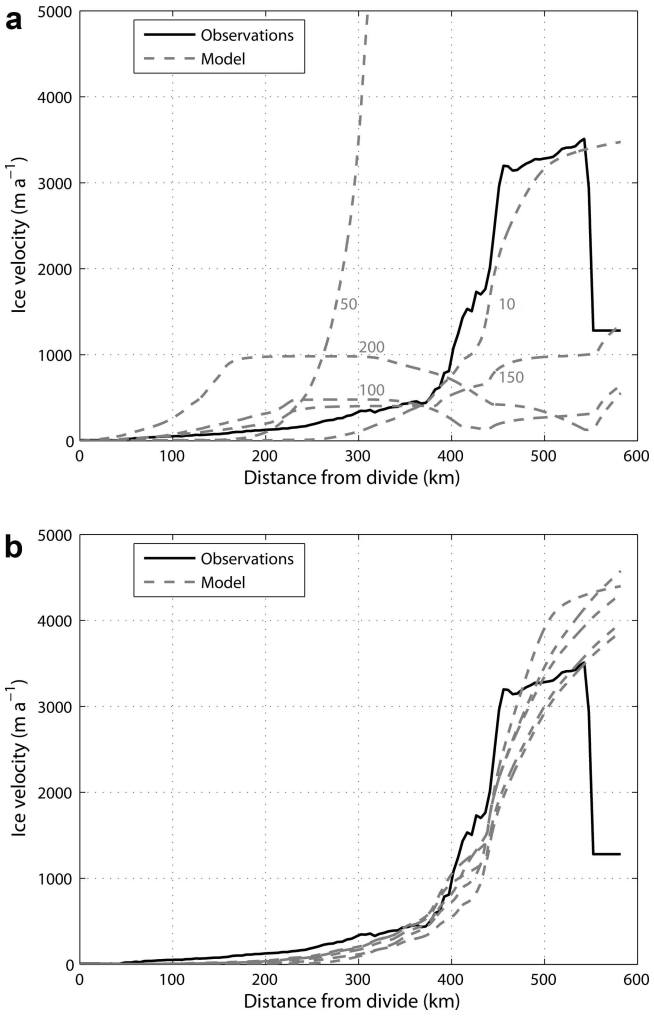

Fig. 5. Modeled velocity profiles of Thwaites Glacier after 10, 50, 100, 150 and 200 years for (a) Exp. CW (labeled) and (b) Exp. VW3 (from left to right). The velocity profile of (a) is truncated at 5000 m a^{-1} to allow comparison with (b).

with a pinning point, which slows the retreat and stabilizes the grounding line. Jamieson and others (2012) found that the grounding-line retreat of Marguerite Bay Ice Stream (MBIS) since the Last Glacial Maximum was interrupted by stabilizations in narrow ice-stream regions caused by both enhanced lateral drag and the mass-conservation principle explained above (ice-sheet thickening), even if the bedrock slope was favorable for unstable behavior. However, MBIS has an average width of ~30 km (with narrow regions of 20 km), while we use a width of 50 km at the calving front increasing up to ~300 km close to the divide in Exp. VW3. Therefore, lateral drag is more important in the work of Jamieson and others (2012) than in our study.

In those same experiments (Exps. VW1–VW3), the mean grounding-line retreat rate (0.3 km a^{-1}) is lower than the observed 1 km a^{-1} (Tinto and Bell, 2011) and the grounding-line thinning rate is comparable with the observations (Shepherd and others, 2010; Pritchard and others, 2012) in the very first years of the simulation, i.e. during the relaxation phase (Fig. 7). Those rates substantially increase and vary in time afterwards, due to the position of the grounding line on a retrograde bed slope. Moreover, the grounding line can slightly readvance (positive migration rates) during the overall retreat process because of the contact between the ice shelf and a pinning point (e.g. between 55 and 60 years) (Fig. 7).

In the experiments where the ice-shelf width is kept constant (Exps. CSW1–CSW3), the grounding line retreats much faster than in the experiments with spatially variable width (Exps. VW1–VW3) and reaches a position of $x_g \approx 220$ km in 200 years, but this retreat is slower than the constant-width experiment (Exp. CW), as shown in Figures 4c and 6. Some stages of slowing down are identified in those three experiments (~60–80 and 100–200 years) and are linked to the grounding line positioned on a bedrock high (Fig. 6), confirming a finding of Parizek and others (2013) for TG. A wider ice shelf ($\omega_{CSW1} > \omega_{CSW2} > \omega_{CSW3}$) gives a slightly more retreated grounding-line position (Fig. 6). Increasing the width in the ice shelf means that the width spatial gradient between the ice sheet and the ice shelf decreases, providing higher flux and less stabilization. The mean grounding-line retreat rate of those experiments is 1.1–1.2 km a^{-1}, closer to the observations than Exps. CW and

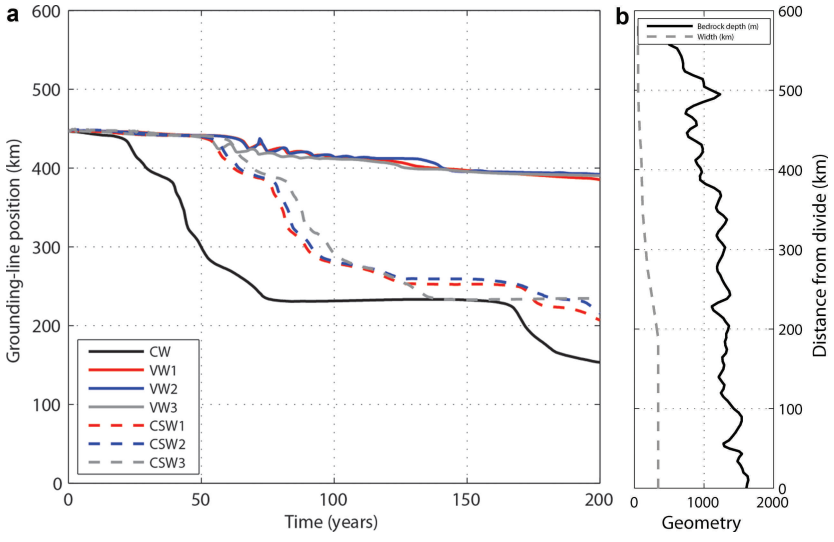

Fig. 6. (a) Thwaites grounding-line position as a function of time for the width experiments. (b) Bedrock depth and VW3 width.

https://doi.org/10.3189/2014JoG13J117 Published online by Cambridge University Press

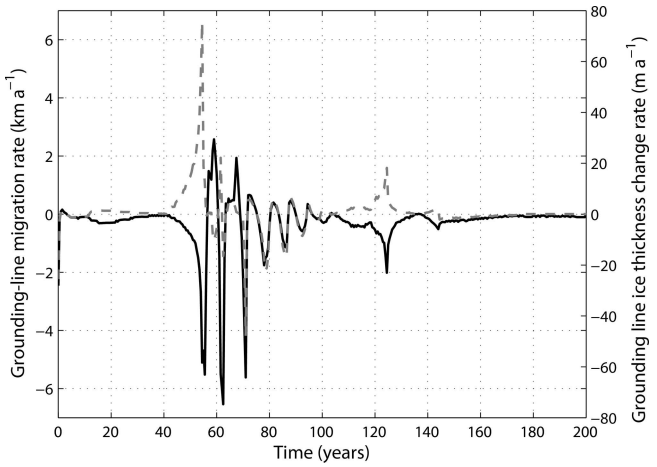

Fig. 7. Grounding-line migration rate (solid black curve) and ice-thickness change rate (dashed gray curve) corresponding to Exp. VW3.

VW1–VW3. However, this parallel-sided case is not necessarily more realistic than Exps. VW1–VW3; as the grounding line retreats, there are prominent highs on either side of the domain that act as pinning points for the new ice shelf, and this is not captured by the model. Therefore, causing the grounding line to retreat with a parallel-sided ice shelf overestimates the vulnerability of TG.

Applying buttressing (experiments starting with 'CF') also reduces the grounding-line retreat compared to Exp. CW (Figs 4d and 8). This can be compared with the results previously obtained by Drouet and others (2013). As a matter of fact, an increase of buttressing effect (through a decrease in C_F) lowers ice flux at the grounding line and therefore provides a slightly more advanced grounding-line position. Furthermore, combining the buttressing increases with VW3 parameterization (variable width) leads to less grounding-line retreat than with CSW1 parameterization (constant shelf width; Fig. 8). An extreme case (CF4VW3; i.e. $C_F = 0.2$) shows a final grounding-line position some kilometers downstream from the observed one. As for the CSW1–CSW3 experiments, bedrock highs tend to stabilize the grounding-line position for some years (Fig. 8).

Using Bedmap2 for the bed (with CSW1 width profile and $C_F = 1$) provides a final grounding-line position of $x_g \approx 440$ km (after 200 years), i.e. on a bedrock high very close to the initial position. This behavior is completely different from Exp. CSW1, which uses the same parameters but not the same bedrock elevation, and is in agreement with the results of Parizek and others (2013). Neither Bedmap2 nor Parizek and others (2013) include the Tinto and Bell (2011) bathymetric model, wich may explain why the grounding line does not retreat as much. Indeed, the slightly different bedrock geometry in the vicinity of the grounding line between both datasets plays a non-negligible role in the behavior of TG. The initial grounding line is located on a small sill in our dataset, but 5 km downstream of this sill in Bedmap2 (Fig. 2).

The final grounding-line positions obtained for all the 16 experiments performed in this study are shown in Figure 9. Four experiments (CW and CSW1–CSW3) lead to a grounding-line retreat of >200 km in 200 years (i.e. mean retreat rate of $\geq$1 km a^{-1}). All simulations show a retreat of the grounding line, except those with high ice-shelf buttressing combined with a non-constant shelf width (CF3VW3 and CF4VW3) and the one including Bedmap2 data. Almost all simulations lead to a contact between the ice shelf and a pinning point. The location of these pinning points is indicated through the color code in Figure 9.

CONCLUSIONS AND OUTLOOK

We computed the short timescale response of TG (200 years) with an SSA flowline ice-stream/ice-shelf model and all the available input data (geometry, ice velocity, basal shear stress, ice temperature, sub-ice-shelf melt rate, accumulation rate). All simulations show a retreat of the grounding line with some stages of slowing down, except two simulations where high ice-shelf buttressing combined with a variable ice-shelf width and the simulation using Bedmap2 data. We identify that the retreat is greatly slowed when the effect of flow convergence is included, i.e. using a variable glacier width in the continuity equation. Therefore, the unstable nature of the bedrock in this region (TG has an overall upward-sloping bedrock) is reduced when taking into account the flow coming from the glacier tributaries. An

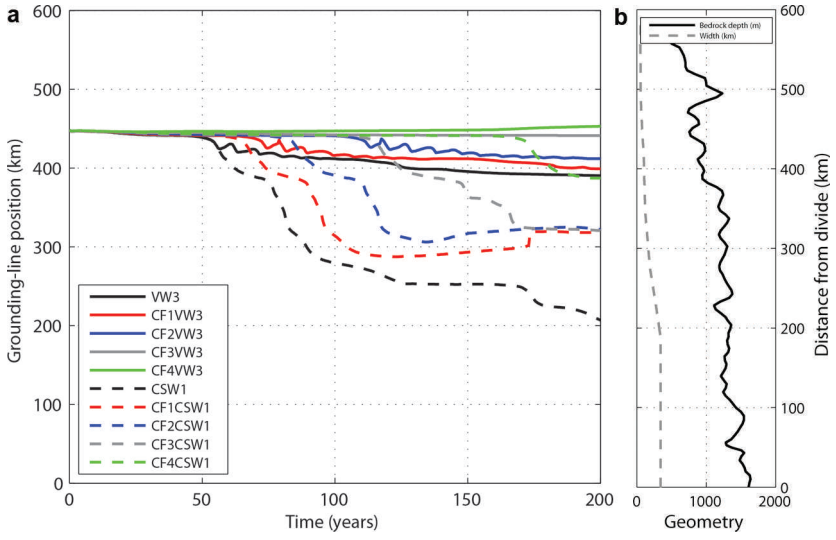

Fig. 8. (a) Thwaites grounding-line position as a function of time for the buttressing experiments. (b) Bedrock depth and VW3 width.

https://doi.org/10.3189/2014JoG13J117 Published online by Cambridge University Press

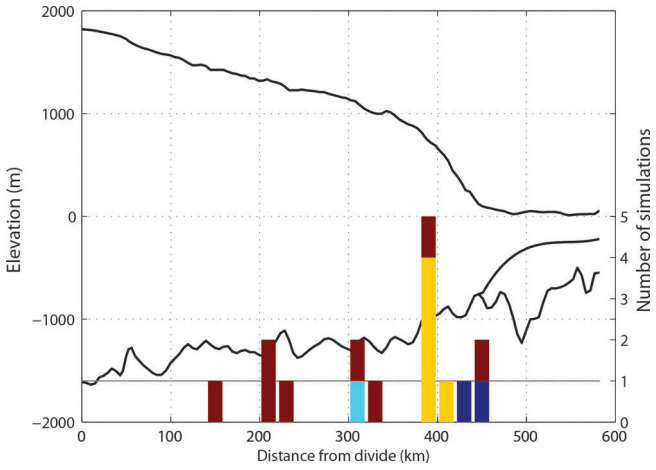

Fig. 9. Observed ice-sheet/ice-shelf geometry of Thwaites Glacier along with a frequency histogram of model simulations binned by final grounding-line position (within a range of 20 km). Blue bars show frequency of 'non-pinned shelf' simulations, while other colors show frequency of 'pinned shelf' simulations, i.e. simulations with an ice shelf in contact with a pinning point (PP) at the end of the simulation (as Gladstone and others, 2012). The different colors indicate where the ice shelf makes first contact with a PP (cyan: PP location ~380 km from the divide; yellow: PP location ~450 km; dark red: PP location ~555 km).

appropriate flowline modeling study should include glacier width, in order to provide reasonable evolution of glacier geometry and grounding-line retreat.

The way the width is parameterized produces different results in terms of grounding-line migration and ice velocity. A convergence in the ice shelf decreases the ice flux and tends to stabilize the grounding line, while a constant ice-shelf width leads to speed up and grounding-line retreat. Moreover, the parameterization of buttressing also affects the grounding-line position. Our experiments show that if we do not take buttressing into account, this can lead to a drastic grounding-line retreat (300 km in 200 years in the constant-width experiment).

These experiments were performed using a flowline model, which considerably reduces the computation time compared with a 3-D model. However, buttressing and width parameterizations used here should be compared with a 3-D model that includes these effects. In this study, we also assume that an SSA model works well for TG as it is a fast-flowing glacier. However, there may be a contribution from vertical shear that could slow down the ice flow. SSA models only include membrane stresses and are faster in their response than models including both membrane stresses and vertical shearing (Pattyn and others, 2013).

ACKNOWLEDGEMENTS

This work was supported by both the IceCube-Dyn project (Actions de recherche concertées) funded by the French Community of Belgium and the ice2sea project funded by the European Commission's 7th Framework Programme through grant 226375 (ice2sea manuscript No. 159). We thank B.R. Parizek, A.M. Le Brocq, K.J. Tinto and I. Joughin for constructive comments and for the provision of data. We also acknowledge helpful clarifications and comments from two anonymous reviewers, and the Scientific Editor H.A. Fricker.

REFERENCES

Bamber JL, Gomez-Dans JL and Griggs JA (2009) A new 1 km digital elevation model of the Antarctic derived from combined satellite radar and laser data – Part 1: data and methods. *Cryosphere*, **3**(1), 101–111 (doi: 10.5194/tc-3-101-2009)

Chen JL, Wilson CR, Blankenship D and Tapley BD (2009) Accelerated Antarctic ice loss from satellite gravity measurements. *Nature Geosci.*, **2**(12), 859–862 (doi: 10.1038/ngeo694)

Cornford SL and 8 others (2013) Adaptive mesh, finite volume modeling of marine ice sheets. *J. Comput. Phys.*, **232**(1), 529–549 (doi: 10.1016/j.jcp.2012.08.037)

Docquier D, Perichon L and Pattyn F (2011) Representing grounding line dynamics in numerical ice sheet models: recent advances and outlook. *Surv. Geophys.*, **32**(4–5), 417–435 (doi: 10.1007/s10712-011-9133-3)

Drouet AS and 6 others (2013) Grounding line transient response in marine ice sheet models. *Cryosphere*, **7**(2), 395–406 (doi: 10.5194/tc-6-1561-2012)

Dupont TK and Alley RB (2005) Assessment of the importance of ice-shelf buttressing to ice-sheet flow. *Geophys. Res. Lett.*, **32**(4), L04503 (doi: 10.1029/2004GL022024)

Durand G, Gagliardini O, Zwinger T, Le Meur E and Hindmarsh RCA (2009) Full Stokes modeling of marine ice sheets: influence of the grid size. *Ann. Glaciol.*, **50**(52), 109–114 (doi: 10.3189/172756409789624283)

Fretwell P and 59 others (2013) Bedmap2: improved ice bed, surface and thickness datasets for Antarctica. *Cryosphere*, **7**(1), 375–393 (doi: 10.5194/tc-7-375-2013)

Gladstone RM and 9 others (2012) Calibrated prediction of Pine Island Glacier retreat during the 21st and 22nd centuries with a coupled flowline model. *Earth Planet. Sci. Lett.*, **333–334**, 191–199 (doi: 10.1016/j.epsl.2012.04.022)

Griggs JA and Bamber JL (2009) Ice shelf thickness over Larsen C, Antarctica, derived from satellite altimetry. *Geophys. Res. Lett.*, **36**(19), L19501 (doi: 10.1029/2009GL039527)

Gudmundsson GH (2011) Ice-stream response to ocean tides and the form of the basal sliding law. *Cryosphere*, **5**(1), 259–270 (doi: 10.5194/tc-5-259-2011)

Gudmundsson GH, Krug J, Durand G, Favier L and Gagliardini O (2012) The stability of grounding lines on retrograde slopes. *Cryosphere*, **6**(6), 1497–1505 (doi: 10.5194/tc-6-1497-2012)

Hellmer H, Kauker F, Timmermann R, Determann J and Rae J (2012) Twenty-first-century warming of a large Antarctic ice-shelf cavity by a redirected coastal current. *Nature*, **485**(7397), 225–228 (doi: 10.1038/nature11064)

Holt JW and 8 others (2006) New boundary conditions for the West Antarctic Ice Sheet: subglacial topography of the Thwaites and Smith glacier catchments. *Geophys. Res. Lett.*, **33**(9), L09502 (doi: 10.1029/2005GL025561)

Jamieson SSR and 6 others (2012) Ice-stream stability on a reverse bed slope. *Nature Geosci.*, **5**(11), 799–802 (doi: 10.1038/ngeo1600)

Joughin I, Abdalati W and Fahnestock MA (2004) Large fluctuations in speed on Greenland's Jakobshavn Isbræ glacier. *Nature*, **432**(7017), 608–610 (doi: 10.1038/nature03130)

Joughin I and 6 others (2009) Basal conditions for Pine Island and Thwaites Glaciers, West Antarctica, determined using satellite and airborne data. *J. Glaciol.*, **55**(190), 245–257 (doi: 10.3189/002214309788608705)

Joughin I, Smith BE and Holland DM (2010a) Sensitivity of 21st century sea level to ocean-induced thinning of Pine Island Glacier, Antarctica. *Geophys. Res. Lett.*, **37**(20), L20502 (doi: 10.1029/2010GL044819)

Joughin I, Smith BE, Howat IM, Scambos T and Moon T (2010b) Greenland flow variability from ice-sheet-wide velocity mapping. *J. Glaciol.*, **56**(197), 415–430 (doi: 10.3189/002214310792447734)

Le Brocq AM, Payne AJ and Vieli A (2010) An improved Antarctic dataset for high resolution numerical ice sheet models

(ALBMAP v1). *Earth Syst. Sci. Data*, **2**(2), 247–260 (doi: 10.5194/essdd-3-195-2010)
MacAyeal DR (1989) Large-scale ice flow over a viscous basal sediment: theory and application to Ice Stream B, Antarctica. *J. Geophys. Res.*, **94**(B4), 4071–4087 (doi: 10.1029/JB094iB04p04071)
MacGregor J, Catania GA, Markowski MS and Andrews AG (2012) Widespread rifting and retreat of ice-shelf margins in the eastern Amundsen Sea Embayment between 1972 and 2011. *J. Glaciol.*, **58**(209), 458–466 (doi: 10.3189/2012JoG11J262)
Nitsche FO, Jacobs SS, Larter RD and Gohl K (2007) Bathymetry of the Amundsen Sea continental shelf: implications for geology, oceanography, and glaciology. *Geochem. Geophys. Geosyst.*, **8**(Q10), Q10009 (doi: 10.1029/2007GC001694)
Olbers DJ and Hellmer HH (2010) A box model of circulation and melting in ice shelf caverns. *Ocean Dyn.*, **60**(1), 141–153 (doi: 10.1007/s10236-009-0252-z)
Parizek BR and 10 others (2013) Dynamic (in)stability of Thwaites Glacier, West Antarctica. *J. Geophys. Res.*, **118**(F2), 638–655 (doi: 10.1002/jgrf.20044)
Paterson WSB (1994) *The physics of glaciers*, 3rd edn. Elsevier, Oxford
Pattyn F and 18 others (2012) Results of the Marine Ice Sheet Model Intercomparison Project, MISMIP. *Cryosphere*, **6**(3), 573–588 (doi: 10.5194/tc-6-573-2012)
Pattyn F and 27 others (2013) Grounding-line migration in plan-view marine ice-sheet models: results of the ice2sea MISMIP3d intercomparison. *J. Glaciol.*, **59**(215), 410–422 (doi: 10.3189/2013JoG12J129)
Pollard D and DeConto RM (2012) Description of a hybrid ice sheet–shelf model, and application to Antarctica. *Geosci. Model Dev. Discuss.*, **5**(2), 1077–1134 (doi: 10.5194/gmdd-5-1077-2012)
Pritchard HD, Ligtenberg SRM, Fricker HA, Vaughan DG, Van den Broeke MR and Padman L (2012) Antarctic ice-sheet loss driven by basal melting of ice shelves. *Nature*, **484**(7395), 502–505 (doi: 10.1038/nature10968)
Rignot E (2008) Changes in West Antarctic ice stream dynamics observed with ALOS PALSAR data. *Geophys. Res. Lett.*, **35**(12), L12505 (doi: 10.1029/2008GL033365)
Rignot E and 6 others (2008) Recent Antarctic ice mass loss from radar interferometry and regional climate modelling. *Nature Geosci.*, **1**(2), 106–110 (doi: 10.1038/ngeo102)
Rignot E, Velicogna I, Van den Broeke MR, Monaghan A and Lenaerts J (2011) Acceleration of the contribution of the Greenland and Antarctic ice sheets to sea level rise. *Geophys. Res. Lett.*, **38**(5), L05503 (doi: 10.1029/2011GL046583)
Scambos TA, Haran TM, Fahnestock MA, Painter TH and Bohlander J (2007) MODIS-based Mosaic of Antarctica (MOA) data sets: continent-wide surface morphology and snow grain size. *Remote Sens. Environ.*, **111**(2–3), 242–257 (doi: 10.1016/j.rse.2006.12.020)
Schoof C (2007) Ice sheet grounding line dynamics: steady states, stability, and hysteresis. *J. Geophys. Res.*, **112**(F3), F03S28 (doi: 10.1029/2006JF000664)
Shepherd A, Wingham D, Wallis D, Giles K, Laxon S and Sundal AV (2010) Recent loss of floating ice and the consequent sea level contribution. *Geophys. Res. Lett.*, **37**(13), L13503 (doi: 10.1029/2010GL042496)
Thoma M, Jenkins A, Holland D and Jacobs S (2008) Modelling circumpolar deep water intrusions on the Amundsen Sea continental shelf, Antarctica. *Geophys. Res. Lett.*, **35**(18), L18602 (doi: 10.1029/2008GL034939)
Tinto KJ and Bell RE (2011) Progressive unpinning of Thwaites Glacier from newly identified offshore ridge: constraints from aerogravity. *Geophys. Res. Lett.*, **38**(20), L20503 (doi: 10.1029/2011GL049026)
Van de Berg WJ, Van den Broeke MR, Reijmer CH and Van Meijgaard E (2006) Reassessment of the Antarctic surface mass balance using calibrated output of a regional atmospheric climate model. *J. Geophys. Res.*, **111**(D11), D11104 (doi: 10.1029/2005JD006495)
Van der Veen CJ and Whillans IM (1996) Model experiments on the evolution and stability of ice streams. *Ann. Glaciol.*, **23**, 129–137
Vieli A and Payne AJ (2005) Assessing the ability of numerical ice sheet models to simulate grounding line migration. *J. Geophys. Res.*, **110**(F1), F01003 (doi: 10.1029/2004JF000202)
Weertman J (1974) Stability of the junction of an ice sheet and an ice shelf. *J. Glaciol.*, **13**(67), 3–11

MS received 23 May 2013 and accepted in revised form 10 January 2014